Chemical Engineering Science 269 (2023) 118490

Contents lists available at ScienceDirect

Chemical Engineering Science

journal homepage: www.elsevier.com/locate/ces

The synergy between substrate architecture of 3D-printed catalytic converters and hydrogen for low-temperature aftertreatment systems

Nikolina Kovacev [a,*], Omid Doustdar [a], Sheng Li [b], Athanasios Tsolakis [a], Jose Martin Herreros [a], Khamis Essa [a,*]

[a] Department of Mechanical Engineering, University of Birmingham, Edgbaston, B15 2TT, United Kingdom
[b] School of Electromechanical Engineering, Guangdong University of Technology, Guangzhou, Guangdong 510006, China

HIGHLIGHTS

- DLP technology was successfully used to manufacture lattice-based substrates.
- 3D-printed lattices showed a superior light-off behaviour for all studied species.
- Hydrogen presence further decreased light-off temperatures in ED and D45.

ARTICLE INFO

Article history:
Received 26 July 2022
Received in revised form 10 January 2023
Accepted 14 January 2023
Available online 18 January 2023

Keywords:
Additive manufacturing
Aftertreatment system
Catalyst
Honeycombs
3D printing

ABSTRACT

This study proposes 3D-printed diamond-based lattice substrates as catalytic converters in the automotive aftertreatment system to improve vehicle cold-start emissions. The study aimed to compare the influence of 3D-printed diamond-based catalyst structures on the light-off behaviour compared to the conventional 400 Cell Per Square Inch (CPSI) honeycomb catalyst design in a real exhaust gas environment. Moreover, the benefits of H_2 addition on the performance of advanced lattice structures are examined for the first time to further increase the low-temperature catalytic efficiency. Digital Light Processing (DLP) technology was effectively utilised to manufacture lattice structures with high cell density to allow a comparison between conventional and advanced geometry designs. Further, the 3D-printed substrates were catalyst coated, and their light-off behaviour was studied in a diesel exhaust environment. The results of the light-off showed a significant improvement in the light-off temperatures for CO, THC and NO in the 3D-printed lattice structures. Furthermore, H_2 presence additionally enhanced the low-temperature activity of the AM lattice structures.

1. Introduction

Stringent legislation to combat the air pollution caused by internal combustion engine exhaust emissions requires the automotive industry to develop more efficient combustion strategies and advanced catalysts for exhaust gas aftertreatment. Advanced catalytic converters in all vehicles are designed to be effectively perform the oxidation of carbon monoxide (CO), oxidation of unburnt and cracked hydrocarbons (THCs), reduction of nitrogen oxides (NO_x) and capture of particulate matter (PM). The critical component in exhaust catalytic converters responsible for the purification of noxious exhaust gases is a flow-through channel structure coated with active material (i.e., honeycomb).

Extrusion is the most widely used method for manufacturing conventional ceramic honeycomb monolith substrates. Consequently, the honeycomb design depends on specially designed dies, limiting the design to simple geometric shapes, such as square, hexagonal, circular or triangular (Avila et al., 2005). Recognition of the honeycomb's limited performance owned to the laminar flow inside the channels (Kim and Son, 1999; Cornejo et al., 2020), hot spots and non-isothermal temperatures in axial and radial directions (Busse et al., 2018) has resulted in extensive research of possible process intensification by direct alteration of the design of the monolith substrate (Papetti et al., 2021). Open cellular foams are attractive candidates for a wide range of heat and mass transfer applications due to their high porosity, high heat conductivity, mechanical strength and feasible radial mixing of the

* Corresponding authors.
E-mail addresses: n.kovacev@bham.ac.uk (N. Kovacev), k.e.a.essa@bham.ac.uk (K. Essa).

https://doi.org/10.1016/j.ces.2023.118490
0009-2509/

fluid (Klumpp et al., 2014; Lucci et al., 2014). However, cellular foams are not commonly employed in automotive applications since the improved mass transfer characteristics have a penalty of an increased pressure drop. Regular arrays of lattice cells were recently found to outperform the randomised foam structure and show a better trade-off between mass transfer and pressure drop (Lucci et al., 2015). Papetti et al. (Papetti et al., 2018) introduced regular polyhedral cell designs inspired by foam structures and manufactured lab-scale samples by stereolithography. Measurements in the model gas reactor confirmed the mass transfer advantages of the polyhedral structures, however low geometric surface area of the manufactured lattices led to a decrease in the light-off behaviour of AM structures in comparison with the traditional honeycomb design. Hajimirzaee et al. (Hajimirzaee and Doyle, 2020; Hajimirzaee et al., 2021) manufactured both lab-scale and industrial-sized lattice substrates based on interconnected rods with repeating angular offset between deposited layers using liquid deposition modelling 3D printing technology. The results showed an indication of superior catalytic efficiency for the 3D-printed samples, however backpressures over the 3D-printed structures were higher than for conventional honeycomb monolith (Hajimirzaee and Doyle, 2020).

Manufacturing constraints have also limited the amount of design freedom in investigations on the additively manufactured (AM) catalyst substrates. In terms of catalyst development for automotive aftertreatment, AM's full potential is yet to be realised. For the processing of ceramics, vat polymerisation technologies based on liquid ceramic suspensions such as Stereolithography (SLA) and Digital-Light Processing (DLP) offer advantageous printing resolution (Santoliquido et al., 2019). Various additive manufacturing techniques have enabled the fabrication of complex ceramic supports for use in HTP thruster applications (Essa et al., 2017; Hassanin et al., 2020), biomedical applications (El-Sayed et al., 2020; Hassanin et al., 2018), oil sensing (Sabouri et al., 2017), and as potential catalytic converters in the automotive sector (Hajimirzaee and Doyle, 2020; Papetti et al., 2018; Santoliquido et al., 2017). By adding materials layer by layer, the creation of complex geometrical shapes in a wide range of materials is facilitated (Hassanin et al., 2021). Bogdan and Michorczyk (Bogdan and Michorczyk, 2020) give an informative state-of-art- review on 3D printing technologies used to fabricate a range of heterogeneous catalysts and supports, and the most recent review study by Zhu et al. (Zhu et al., 2022) highlights the common catalyst 3D printing strategies that mainly include extrusion-based, vat photopolymerisation-based strategies and powder-based strategies.

The ability of compression ignition engines to operate under lean in fuel conditions (high air/fuel ratios) leads to high fuel economy, but also to low exhaust gas temperature and the presence of oxygen in the exhaust which challenge catalytic emission control. Cold-start and engine stop-start have been brought up as a significant concern in the reduction of THC and CO emissions under a tighter regulatory environment (Olabi et al., 2020). Vehicle thermal management solutions including thermochemical exhaust gas waste heat fuel reforming have shown great potential in improving the low-temperature performance of the aftertreatment systems (Herreros et al., 2014; Umar et al., 2021; Megaritis et al., 2010). Exhaust gas fuel reforming provides small concentration of hydrogen (H_2) to the aftertreatment catalyst enhancing their performance (Azis et al., 2015; Herreros et al., 2014; Theinnoi et al., 2018). For instance, H_2 has a beneficial influence on CO, hydrocarbons and NO oxidation over various diesel oxidation catalysts (Herreros et al., 2014).

In addition, the structure of the monolith substrate can be designed to improve the low temperature catalyst performance. We recently reported that diamond-based lattice structures show great potential as substituents for a traditional channel design based on numerical simulation of the fluid flow and heat transfer in a non-reactive environment (Kovacev et al., 2020). However, the effect of H_2 on the performance of advanced catalytic designs, such as lattice structures, has not been reported yet. In the present paper, novel ceramic diamond-based lattice structures are manufactured via DLP additive manufacturing technology, functionalised with catalytic coating, and tested for effectiveness in a real exhaust gas environment. Lattice structures that exhibit similar cell density as the conventional honeycomb and high specific surface area were employed to allow a fair comparison. Therefore, the study aims to compare the influence of the innovative 3D-printed diamond-based catalyst structures on the light-off behaviour compared to the benchmark 400 CPSI honeycomb catalyst design under real exhaust gas conditions. Additionally, recent studies have been already reported using promoters like hydrogen (H_2) on CO and HCs oxidation and NO_2 formation (Herreros et al., 2014). This study also aims to find potential synergetic effects of the interaction between lattice structures and the addition of hydrogen for the first time under real exhaust engine conditions to increase the low-temperature catalytic efficiency further. Findings from this study on 3D-printed lattice can be implemented in all catalytic converter systems of all commercial and Hybrid Electric Vehicles (HEV) to meet stringent emissions legislation and enrich the research on moving toward low-emissions vehicles.

2. Experimental

2.1. Substrate design

Diamond unit cell was chosen as the basis for the design of the lattice substrates as it has shown excellent performance in other catalytic applications (Essa et al., 2017) and has demonstrated thermal and hydraulic advantages over the 400 CPSI honeycomb (HC) based on numerical simulations in a non-reactive environment (Kovacev et al., 2020). A diamond lattice has an isotropic geometry consisting of four struts connected nodally with another four struts. A diamond cell with a strut orientation angle (θ) of 45°, referred to as D45, is depicted in Fig. 1a). The elongated diamond unit cell design is shown in Fig. 1b). This structure results in struts that are aligned with the incoming flow, due to the lower strut orientation angle of 20°, which is expected to reduce the aerodynamic resistance. Based on its wide usage as catalyst support, the 400 CPSI honeycomb monolith design shown in Fig. 1c) is chosen to provide a baseline case (Ibrahim et al., 2018; Piqueras et al., 2021). The lattices were designed to have similar CPSI as the benchmark 400 CPSI HC. The geometric surface area of the substrates was estimated based on the generated CAD model. Geometrical features of the sintered AM samples: diameter (D), length (L), geometric surface area (S_v), porosity (ε), pore diameter (d_p), cell length (L_c), wall thickness (d_w) and strut diameter (d_s) confirmed by SEM are listed in Table 1. The overall dimensions (D and L) of the sintered samples were measured by Vernier Caliper.

2.2. Digital light processing

The ceramic substrates were manufactured using Al_2O_3 photopolymerisable ceramic slurry with optimised rheology and curing characteristics for printing lattice structures (Kovacev et al., 2022). Aluminium oxide powder (A16 SG, Almatis GmbH, Ludwigshafen, Germany) was chosen as the ceramic filler. The as-received ceramic powder was first pre-treated with ethanol and 2 wt% of dispersant to the powder content, followed by planetary ball milling. The mixture was dried first in air and then in an oven to allow solvent evaporation. The resin preparation consisted of

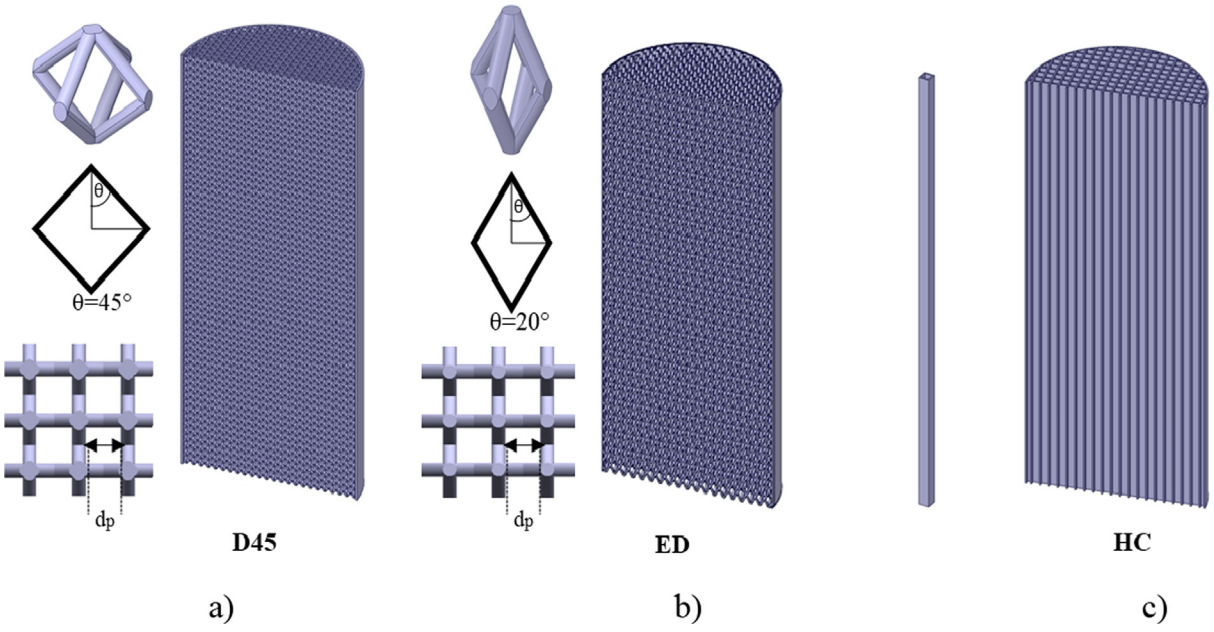

Fig. 1. CAD designs of the studied substrates a) Diamond (D45) b) Elongated Diamond (ED) c) Honeycomb (HC).

Table 1
Geometrical parameters of the 3D-printed sintered substrates.

Substrate	D (mm)	L (mm)	S_v (m^{-1})	ε (-)	d_p (mm)	d_s (mm)	d_w (mm)	L_c (mm)
D45	25	60	2300	0.78	0.95	0.30	–	–
ED	25	60	2000	0.83	0.95	0.30	–	–
HC	25	60	2890	0.68	–	–	0.20	0.95

combining polyfunctional and monofunctional monomers together with a plasticiser. Diphenyl (2,4,6-trimethylbenzoyl) phosphine oxide (Sigma Aldrich, Gillingham, UK) was added to initiate the polymerisation reactions. The pre-treated powder was incrementally added to the resin–photoinitiator mixture until a solid loading of 83 wt% was achieved and the slurry was thoroughly mixed in a turbula mixer overnight (Kovacev et al., 2021). The printing experiments were conducted on the Admaflex 130 (Admatec Europe BV, Alkmaar, The Netherlands). Admaflex technology is based on Digital-Light Processing (DLP), and it applies a "bottom-up" printing approach using a Digital Micromirror Device (DMD) which comprises an array of mirrors, where each mirror represents a single pixel. The exposed layers are irradiated by DLP irradiation throughout the glass bottom. The printing process is as follows: the platform first descends until the distance between the platform and the slurry layer equals one-layer thickness, and the light projects the first slice of information to the slurry layer. The illuminated suspension is cured for several seconds. When the first layer is cured and adhered to the platform, the platform is then lifted by a distance equal to one-layer thickness to achieve one-layer thickness between the first cured layer and the slurry layer. The second layer is then illuminated, cured, and adhered to the first cured layer. This process is repeated until the green body is wholly fabricated. The exposure parameters, layer thickness and orientation, were chosen based on experience and previous resolution studies to achieve the final products of satisfactory accuracy (Kovacev et al., 2021). The overall dimensions of the CAD models were rescaled to compensate for part shrinkage during thermal postprocessing of approximately 14% in lateral and 19% in the vertical direction. Considering over curing, scattering, and sintering shrinkage in the lateral direction, it was necessary to project an image of 0.24 mm for lattice strut diameter and 0.25 mm for honeycomb walls to achieve structures with sintered strut diameter/wall thickness of around 0.3 mm, and 0.2 mm, at an energy density of 42 mJ/cm^2 and 20.16 mJ/cm^2, respectively. The lattice structures were printed in the horizontal direction (XY) in respect of the building axis (Z), with a 45° rotation of the Y-axis, energy density of 42 mJ/cm^2 and layer thickness of 25 μm. The honeycomb was printed in a vertical direction (Z) with an energy density of 20.16 mJ/cm^2 and layer thickness of 50 μm. The uncured slurry trapped in the green parts was cleaned by immersing the green pieces in an ultrasonic bath filled with dibasic ester (Sigma Aldrich, Gillingham, UK). The manufactured samples were then dried by the compressed air stream, debinded and sintered.

2.3. Catalyst preparation and washcoating

The incipient wetness method was used to prepare the catalytic powder for washcoating. Gamma-alumina (γ-Al_2O_3, Sigma Aldrich, Gillingham, UK) powder was used as the catalytic carrier. Firstly, the water capacity of the support material was determined to find out the exact quantity of water needed to dissolve the metal salts. The γ-Al_2O_3 powder was titrated with distilled water to find the support pore volume. Distilled water was added dropwise with a pipette until the powder was fully wet and no excess water was present. The γ-Al_2O_3 powder was then catalytically activated with the metal precursors. An aqueous solution of palladium (II) nitrate hydrate (Sigma Aldrich, Gillingham, UK) and tetraammineplatinum (II) nitrate (Sigma Aldrich, Gillingham, UK) with a weight ratio of 1:1, to achieve a theoretical PGM loading of 2.5 wt% was prepared. The noble metal precursors were weighed and dissolved in the same volume of distilled water required to fill the pores of the support, previously determined by the titration method. The noble metals salt-water mixture was first stirred for 1 h and afterwards

added dropwise to the Al_2O_3 carrier, continuously stirring the powder to achieve complete liquid adsorption. The prepared paste was dried overnight in atmospheric conditions, followed by dying in a furnace at 70 °C and subsequent calcination at 600 °C for 4 h (Gremminger et al., 2020). The washcoating slurry was prepared by mixing 17 wt% of the prepared catalyst powder with deionised water and 5 wt% of dispersant (BYK-180, BYK Chemie, GmbH, Wesel, Germany), with respect to the total mass of the slurry. The mixture was stirred on a magnetic stirrer, followed by planetary ball milling to achieve a homogeneous distribution of the powder in the solution. 5 wt% of boehmite (Disperal, Sasol Germany GmbH, Hamburg, Germany) was added into the mixture to improve the catalyst adherence to the walls of the AM support. The outside walls of the 3D-printed substrates were wrapped in Teflon tape to limit the coating to the lattice/ honeycomb structure. The AM samples were coated with the identical slurry in the same batch. The substrates were immersed vertically into the catalyst slurry and placed under a vacuum for 2 min. The excess slurry was removed with pressurised air. After dip-coating, the excess slurry was removed with pressurised air, and the sample was dried in an oven at 120 °C for one hour. The dip-coating and oven-drying procedure were repeated several times. Overall, 8–12 dip-coating and oven-drying cycles, depending on the substrate structure, were required to achieve the loading of approximately 120 g/ft^3. Finally, the washcoated samples were calcined at 750 °C for 2 h with a ramp rate of 10 °C/min. The catalysts were thermally conditioned in a furnace at 550 °C for 4 h before the experiments with real exhaust gas.

2.4. Catalyst characterisation methods

A series of characterisation experiments were conducted after the catalyst powder was prepared to assess the performance. X-ray diffraction (XRD) of the catalysts was performed via AXRD Benchtop Powder Diffraction System (Proto Manufacturing, Michigan, USA) diffractometer. The intensity of scattered X-rays was measured in a 2θ-range of 20-90°. The morphology of the bare and coated samples was analysed using scanning electron microscopy (TM3030 Tabletop SEM, Hitachi High-Technologies, Tokyo, Japan). The Energy-Dispersive X-ray Spectroscopy (EDS) (JCM-6000, JEOL ltd., Japan) was employed to verify and quantify the elemental composition of the catalyst powder in terms of the atomic percentage. The atomic ratios for the powdered catalyst were obtained at four different areas, and an average value is reported. The Brunauer-Emmett-Teller (BET) surface area of the bare Al_2O_3 support powder and prepared catalytic powder was determined using Micromeritics TriStar II 3020. The samples were degassed for 3 h at 250 °C before the analysis to remove any volatile adsorbates on the surface.

2.5. Engine test procedure

The catalyst washcoated 3D-printed substrates were studied in a single-cylinder research diesel engine exhaust gas to observe the influence of the substrate geometry on the conversion efficiencies of emissions. The engine technical data and specifications are given in Table 2. Standard engine test rig instrumentation to monitor intake air, temperatures (oil, air, inlet manifold and exhaust) and pressures were included in the test rig. The engine was fuelled with ultra-low sulphur diesel (ULSD) provided by Shell Global Solutions UK. The temperatures at the exhaust manifold, before the DOC, after the DOC and at other engine set-up parts were recorded using K-type thermocouples and a Pico Technology TC-08 thermocouple data logger. The engine condition was kept constant in all tests to reduce test-to-test variability and ensure steady-state operation. For this purpose, the coefficient of variation (COV) of the IMEP for 100 cycles was monitored and kept below 4 % during the experiments. The engine was operated at a rotational speed of 1500 rpm with an engine load of 2 IMEP to reproduce low-load driving conditions (Hamedi et al., 2021).

The detailed testing condition and engine-out emissions repeatability are listed in Table 3. The catalyst was placed in a tubular Carbolite Gero furnace with a temperature increase from 100 °C to 400 °C with a heating temperature ramp of 3 °C/min. Gas hourly space velocity (GHSV), defined as the volumetric flow rate of the exhaust gas divided by the external volume of the monolith catalyst, was kept constant at around 33,000 1000 h^{-1}. An MKS MultiGas 2030 FTIR analyser was used to measure gaseous exhaust emissions. The sampling lines were kept at a temperature of 191 °C to limit any water and hydrocarbon condensation and prevent any reaction between exhaust gas species in the line. A Testo 340 flue gas analyser equipped with an oxygen sensor, was used to measure oxygen exhaust content. Engine-out exhaust species concentrations were measured at the beginning and end of each experiment to monitor the repeatability of the exhaust gas composition during the test. Throughout the experiments, the DOC outlet exhaust gas concentration evolution was continuously recorded to calculate the conversion efficiency based on the inlet concentration. The tests were in good agreement and had high repeatability in emissions, and hence in conversion efficiency. Light-off experiments were repeated two times to check the constancy and repeatability of the results. To study the influence of hydrogen, pure H_2 from a gas cylinder purchased from BOC was introduced upstream of the DOC at a concentration of 1000 ppm. A Bronkhorst digital mass flow controller, EL-Flow, is used to measure and control hydrogen injection preciously. The concentration of hydrogen was measured both upstream and downstream of the catalyst by sampling the gas stream using V&F HSense. Fig. 2 illustrates the schematic diagram of the experimental configuration.

Table 2
Test engine specifications.

Engine Specification	Data
Number of Cylinders	1
Bore	84 mm
Connecting Rod Length	160 mm
Displacement Volume	499 cc
Compression Ratio	16.1:1
Maximum Injection Pressure	1500 bar

3. Results and discussion

3.1. Catalyst characterisation

The diffraction pattern of bare γ-Al_2O_3 support and calcinated bimetallic powder is presented in Fig. 3. X-ray diffraction (XRD) patterns of γ-Al_2O_3 support and the bimetallic powder showed a

Table 3
Engine output emissions concentration.

Emissions	Concentration
CO (ppm)	271 ± 20
THC (ppm)	305 ± 69
NO (ppm)	215 ± 9
NO_2 (ppm)	61 ± 3
NO_x (ppm)	275 ± 8
N_2O (ppm)	0.68 ± 0.03
CO_2 (%)	4 ± 0.04
H_2O (%)	4.7 ± 0.21

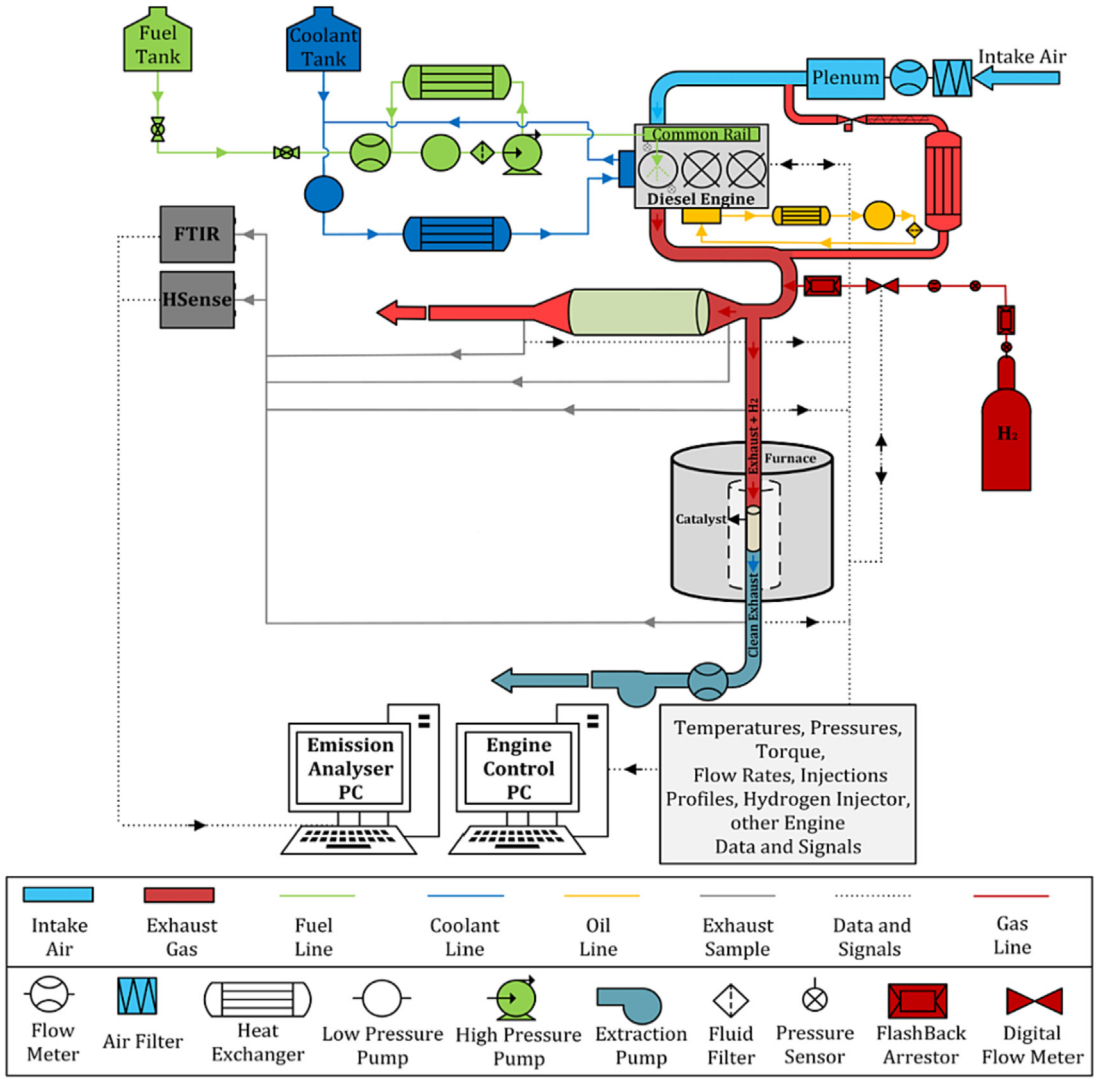

Fig. 2. Schematic diagram of the experimental setup.

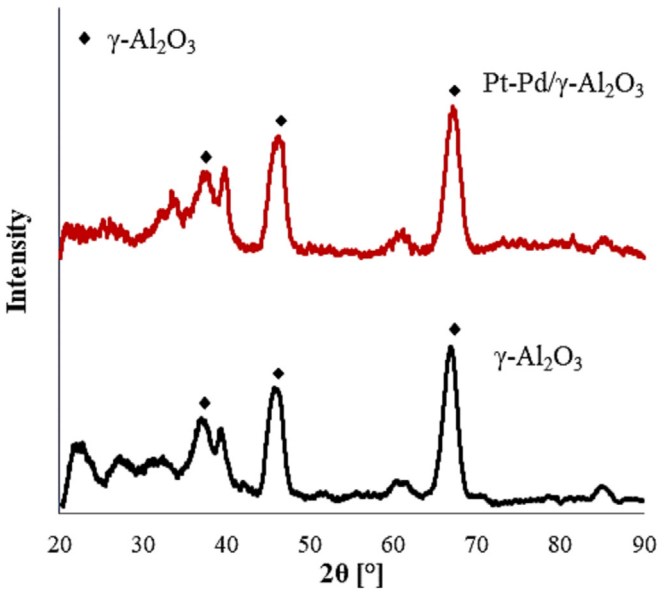

Fig. 3. XRD of the bare gamma-alumina powder and bimetallic powder sample.

very similar profile, with the diffraction peaks attributed to γ-Al_2O_3. Since the XRD peaks for Pt and Pd mainly overlapped with those of γ-Al_2O_3, it was not possible to distinguish any clear peaks associated with the presence of Pt and Pd. The literature suggests that this occurs due to the low content of Pt and Pd and good particle dispersion (Bai et al., 2015; Hajimirzaee and Doyle, 2020). Fig. 4 shows the calcinated, washcoated AM catalysts. The SEM images in Fig. 5 show an example of a) bare lattice and b) the washcoated lattice. The SEM of the calcinated washcoated samples revealed that the inherent surface of the 3D-printed substrate disappeared, presenting substrate coverage by the catalytic coating (Fig. 5b)). Energy dispersive spectroscopy (EDS) showed that the powdered catalyst was composed of Pt, Pd, Al and O. Meanwhile, the average atomic percentages of Pt, Pd, Al and O were determined to be 0.1 %, 0.1 %, 32.2 % and 67.6 %, respectively.

BET analysis revealed the starting Al_2O_3 powder had a BET surface area of 173 m^2/g, whereas, after impregnation with Pd and Pt, the BET surface area of the catalyst powder slightly decreased to the value of 156 m^2/g, most likely due to the impregnation of the active metals on the support and the high calcination temperature employed at 750 °C (Karatzas et al., 2011). All calcinated washcoated samples had washcoats that were resistant to disintegration during handling and experimental testing. High adherence of the

Fig. 4. Washcoated catalysts a) D45 b) ED c) HC.

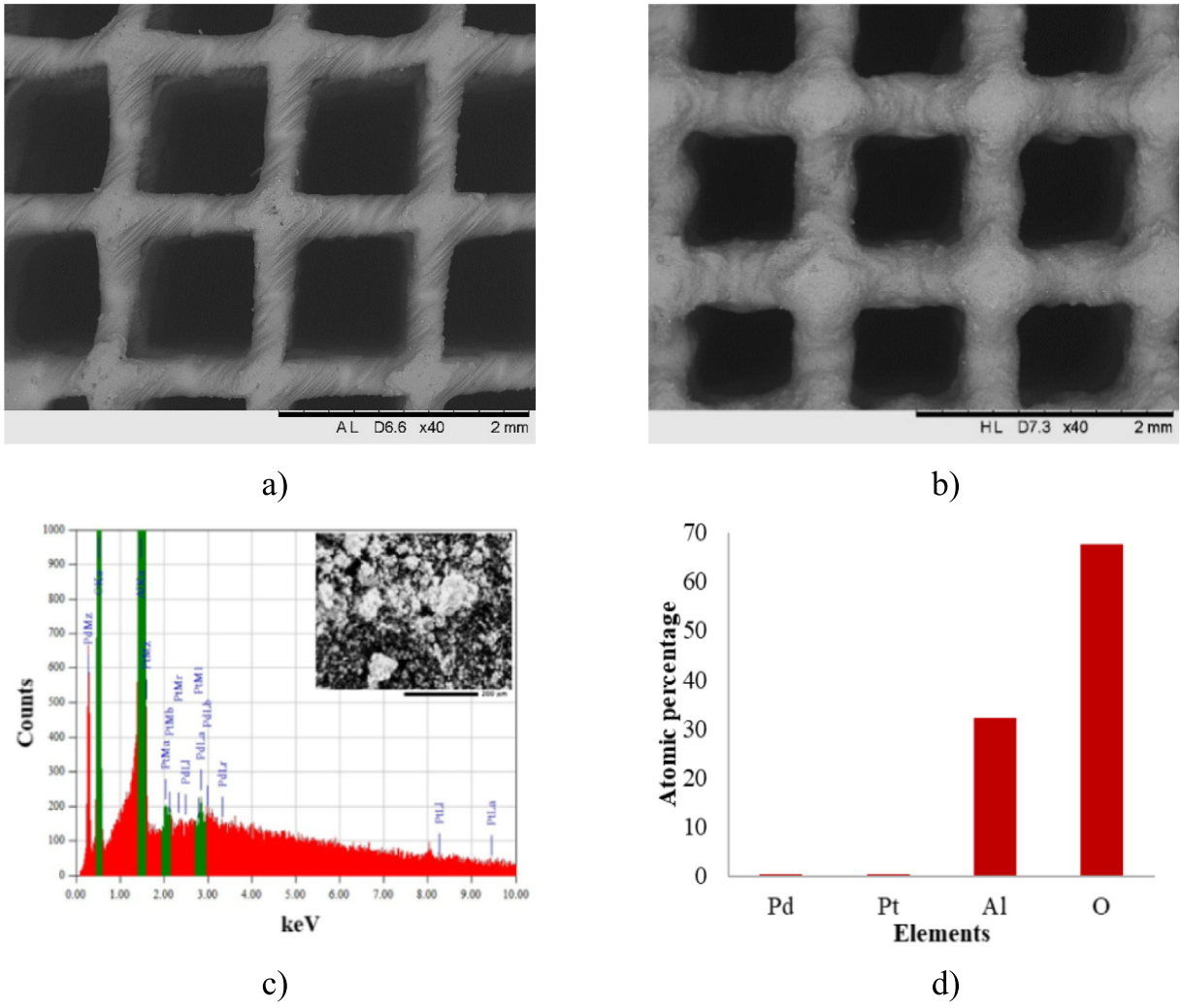

Fig. 5. Exemplary SEM images of a) Bare 3D-printed sample (D45) b) Coated sample (D45) c) EDX spectrum and d) Summary of the Pt-Pd/γ-Al_2O_3 catalyst.

washcoat to the substrate is critical to avoid detachment of the washcoat in severe operating circumstances such as hot exhaust gases at high velocity or mechanical vibrations, which could result in a decrease in catalyst performance (Agrafiotis et al., 1999). The mechanical resistance of the coated layers onto the 3D-printed substrates was evaluated by weighing the coated samples before and after the light-off experiments. In all cases, the adherence of the catalytic layer to the substrates was very good, with weight

losses lower than 1 %. A catalyst substrate comparison in terms of reactivity should involve substrates with the same washcoat amount, the same quantity of active metals, and the same available surface area for the reactions (Lucci et al., 2015). For all substrates, the washcoat composition and the composition and quantity of the active precious metals have been kept identical since they were coated in the same batch of the washcoating slurry. Thus, the reaction behaviour of the catalyst is comparable. The coating method is vital for catalytic applications; determining catalyst performances and homogeneous coating of 3D-printed intricate substrates is often tricky due to the tortuous support geometry (Giani et al., 2006). Considering future research, the coating aspect should be further optimised for coating 3D-printed structures.

3.2. Influence of the substrate structure on the catalyst activity

The performance of the prepared catalytic converters in the real engine exhaust versus temperature for CO, THC, NO (Fig. 6) and the ratio of NO_2/NO_x (Fig. 7) are analysed for the lattices and the reference honeycomb with and without the addition of hydrogen (H_2). Table 4 compares T_{25}, T_{50}, T_{75} and T_{90} values (temperatures recorded for 25 %, 50 %, 75 % and 90 % conversion efficiency levels of CO and THC) for the studied structures, with and without H_2. Conversion curves of all studied structures showed similar light-off trends for all species with the increasing temperature: low conversion at low temperatures, then ignition and ultimately, a plateau where the conversion is no longer influenced by the temperature. Fig. 6a) illustrates the conversion efficiency of the lattices and honeycomb in terms of CO oxidation. In the inlet gas temperature range of 100–150 °C, there is already a clear difference between the reactivity of the studied structures. With the increase of the inlet temperature, the conversion exponentially increases for all structures. The D45 light-off curve revealed a 23 % lower light-off temperature than the honeycomb and the best low-temperature performance among the studied structures. The catalytic efficiency of the ED structure was lower in comparison with D45, due to the 13 % lower surface area. However, the lack in the surface area for ED does not seem to be detrimental for its light-off performance, as the structure achieves superior low-temperature activity compared to the honeycomb. Since the lattice structures have 20–30 % lower surface areas compared to the honeycomb, the superior catalytic activity of the lattice designs implies that the flow regime inside the substrates is more significant than the surface area as the surface area is utilised more efficiently in the 3D-printed substrates. The differences in the activity of the two lattice substrates (D45 and ED) could be explained by their distinct designs resulting in different gas flow paths. Moreover, both D45 and ED also demonstrated 100 % CO conversion at lower temperatures.

A promoting effect of H_2 added upstream of the catalyst on the CO light-off temperature (T_{50}) can be observed for all structures (Table 4). The overall conclusion of conversion efficiency for CO with H_2 remained consistent (D45 > ED > HC). The improvement in the CO conversion in the ED structure with H_2 is remarkable. It is evident that the lower surface area of ED is the reason behind the overall lower catalytic efficiency in comparison with D45. However, the reductions in temperatures recorded for 25 %, 50 %, 75 % and 90 % CO conversion, thanks to H_2 addition, were the highest for the ED structure. This may be related to the higher average gas contact time with the catalyst adhered to the struts of the ED lattice, as lower overall velocity within the lattice struts is expected for this specific structure (Kovacev et al., 2020). The differences between the inlet and outlet gas temperatures at inlet temperatures of 100 °C, 250 °C and 400 °C are presented in Table 5. The thermal properties of both lattice structures are significantly higher than for honeycomb at all temperatures. The superior catalytic activity of the catalysts with H_2 addition at low temperatures cannot be related to H_2 oxidation since H_2 depletion starts only after the majority of CO is already converted (Salomons et al., 2006).

Higher temperature in ED evidence this structure's superior thermal response in comparison with HC and D45, which thanks to the presence of H_2, offsets the drawbacks of the reduced surface area. Fig. 6b) shows THC conversion efficiency. The THC conversion started after a large amount of CO became oxidised in all three structures, when more catalytic active sites became available for hydrocarbons to adsorb onto. Therefore, the trend in the activity (D45 > ED > HC) remained identical to the trend in CO conversions. The peak THC conversion efficiency did not reach 100 % in lattices nor in the HC. This phenomenon has been previously ascribed to the presence of certain long-chain hydrocarbons that contribute to the partial conversion of THC due to their lower diffusivity to reach the catalyst active sites, resulting in incomplete conversion, and it is consistent with our experimental observations (Herreros et al., 2014). The THC light-off temperature was decreased for all structures in H_2 presence. However, the maximum conversion efficiency improvement was not observed for any of the structure. NO conversion efficiency is depicted in Fig. 6c). D45 reached a maximum of 40 % NO conversion, ED 25 %, while the conventional HC structure reached 7 %. Most of the NO is converted to NO_2 which could be used for passive continuous regeneration of a downstream diesel particulate filter (DPF) or to enhance the fast-SCR reaction (Herreros et al., 2014), conventionally at the temperature range between 300 °C and 400 °C, (Jung et al., 2019; Russell and Epling, 2011). In the presence of H_2 in the case of D45, a slight impact on the NO conversion was observed only at moderate temperatures (Fig. 6c)). At higher temperatures, NO conversion diminished. The D45 structure showed the highest overall NO_2 yield in the moderate to the high-temperature range, without the H_2 addition. The addition of H_2 positively affected NO conversion for both HC and ED.

The NO_2/NO_x yield (Fig. 7) for both lattice substrates was greater than in the conventional HC at moderate and high temperatures. At low temperatures, NO_2 is consumed as an oxidant by hydrocarbons and CO, hence the ratio decreases. As the temperature rises, hydrocarbons begin reacting with molecular oxygen, resulting in an increase in NO conversion and consequent NO_2 concentration for all structures. An increase in NO_2/NO_x ratio for the D45 sample at temperatures above 220 °C implies a relatively large selectivity for NO_2 production in this specific structure. However, the ratio started decreasing at high temperatures, which may be explained by the NO to NO_2 oxidation reaction becoming equilibrium limited (Resitoglu et al., 2015). The configurations with the greatest CO and THC conversions were also the ones with the highest NO_2/NO_x ratio illustrating the relations between these exhaust species, also reported in the literature (Lefort et al., 2014). H_2 presence was found to enhance the maximum NO_2 yield in the ED lattice, which may be rationalised by the increased gas-catalyst contact time (Kovacev et al., 2020).

4. Conclusions

The scope of this research work was to demonstrate the potential of additively manufactured lattice-based monolithic substrates as catalytic converters. The lattice-based substrates were manufactured using DLP technology and were successfully coated with bimetallic Pt-Pd catalyst supported on γ-Al_2O_3. Furthermore, their light-off behaviour was tested in the exhaust gas environment. In addition, the benefits of hydrogen addition on lattice performances were explored.

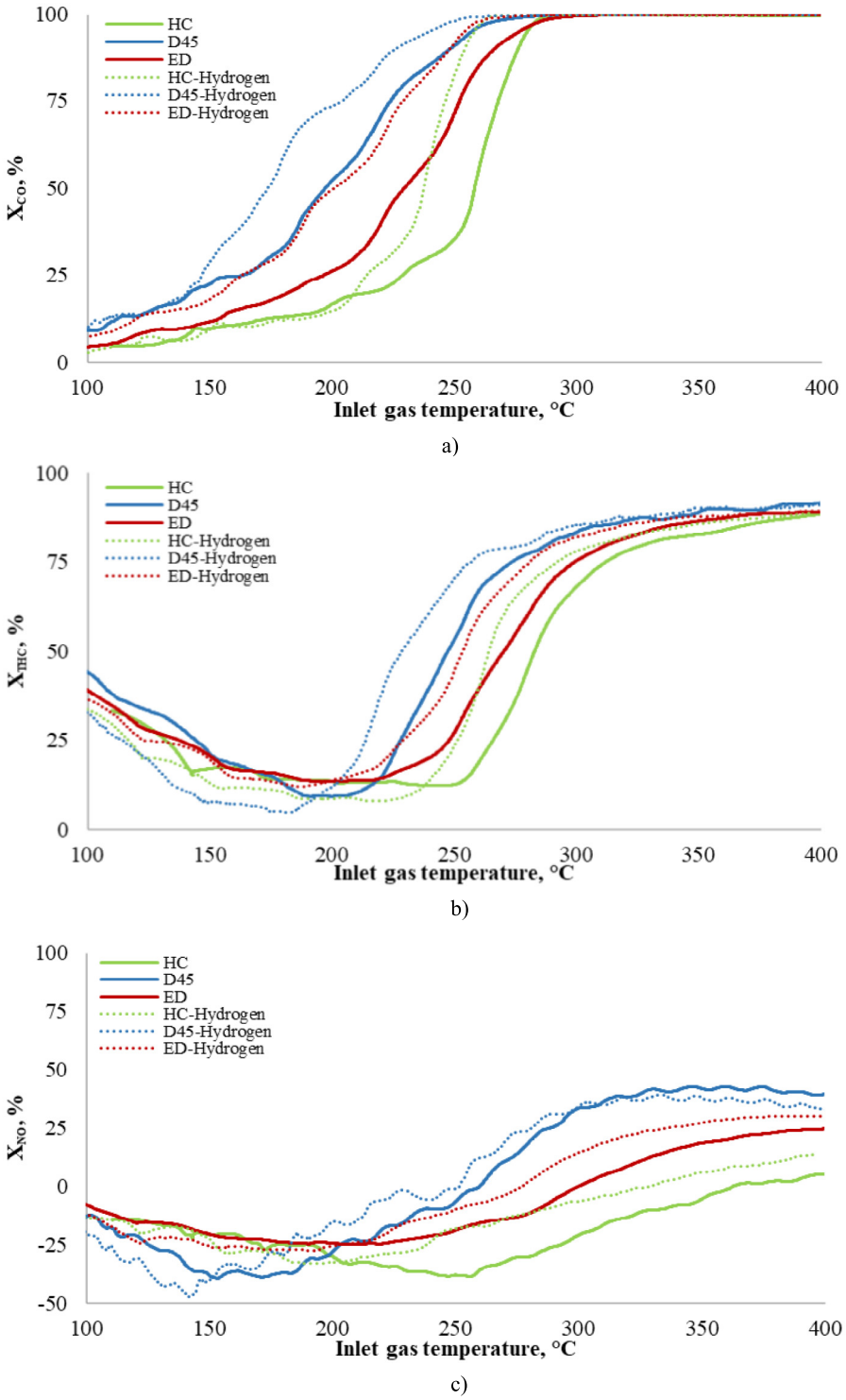

Fig. 6. Conversion efficiencies for a) CO b) THC c) NO for HC, D45 and ED with and without H_2.

The results support the following conclusions:

- DLP technology was successfully used to manufacture intricate lattice-based substrates
- The 3D-printed lattices with a similar cell density as the conventional 400 CPSI HC showed a superior light-off behaviour for all studied species. Both lattice designs overcame the performance of the reference HC catalyst, with H_2 additionally boosting their conversion efficiency.
- The addition of hydrogen to all substrates positively affected the CO light-off temperature; however, the gain in THC light-off temperature reduction was apparent to a lesser extent.
- D45 showed the highest overall NO_2 yield in the moderate to the high-temperature range, regardless of the hydrogen presence
- Hydrogen addition improved the NO_2 production in the ED lattice, possibly due to the unique structure of ED with increased flow residence time, which seems to be more prominent in enhancing the oxidation of the slow chemical reaction of NO to NO_2 with hydrogen.

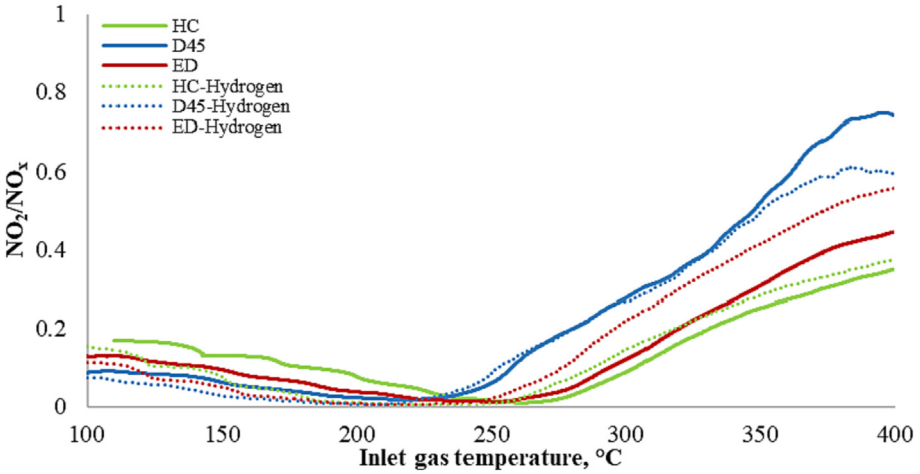

Fig. 7. NO_2/NO_x ratio for HC, D45 and ED, with and without H_2.

Table 4
Summary of T_{25}, T_{50}, T_{75} and T_{90} for CO and THC.

Catalyst	CO				THC			
	T_{25}, °C	T_{50}, °C	T_{75}, °C	T_{90}, °C	T_{25}, °C	T_{50}, °C	T_{75}, °C	T_{90}, °C
HC	220	252	258	263	258	273	300	399
HC-H_2	207	233	240	244	244	258	283	390
D45	154	193	221	244	225	242	267	346
D45-H_2	146	172	200	223	212	226	255	337
ED	186	223	247	259	242	262	291	376
ED-H_2	160	195	223	241	223	248	273	344

Table 5
Difference in the inlet and outlet temperature under hydrogen addition.

Inlet gas temperature	HC	D45	ED
100 °C	13 °C	19 °C	21 °C
250 °C	50 °C	68 °C	71 °C
400 °C	80 °C	95 °C	104 °C

- In combination with hydrogen addition, the intricate lattice structures allowed greater contact of the reactant with the catalyst adhered to the structure's struts, with improved gas–solid contact due to flow mixing and more efficiently used surface area, shifting the light-off curves of all studied species to lower temperatures.

The AM structures described in this paper for DOCs would also be applicable for catalytic converters in other applications, particularly for HEV aftertreatment systems. The findings for the two distinct 3D-printed substrates discussed in this work suggest that an appropriate substrate may be designed based on the application requirements. Furthermore, the structure may be altered to create even more complex designs, such as gradient structures with radial or axial cell density variation or combinations of the two. In addition, the 3D printing material can also be varied to control the substrate's thermal response further. This research proved the importance of 3D printing to design and produce efficient advanced catalytic converters for minimisation of CO, THC, NO_x, and other species to meet stringent emissions regulations and a way forward to low-emissions vehicles.

CRediT authorship contribution statement

Nikolina Kovacev: Conceptualization, Methodology, Data curation, Writing – original draft. **Omid Doustdar:** Methodology, Investigation, Writing – review & editing. **Sheng Li:** Writing – review & editing. **Athanasios Tsolakis:** Writing – review & editing. **Jose Martin Herreros:** Writing – review & editing. **Khamis Essa:** Writing – review & editing, Supervision.

Data availability

Data will be made available on request.

Declaration of Competing Interest

The authors declare that they have no known competing financial interests or personal relationships that could have appeared to influence the work reported in this paper.

Acknowledgements

The research leading to these results has received funding from the Engineering and Physical Sciences Research Council for project FACE - Novel Integrated Fuel Reformer-Aftertreatment System for Clean and Efficient Road Vehicles under grant number EP/P031226/1.

References

Agrafiotis, C., Tsetsekou, A., Ekonomakou, A., 1999. Effect of particle size on the adhesion properties of oxide washcoats on cordierite honeycombs. J. Mater. Sci. Lett. 18 (17), 1421–1424.
Avila, P., Montes, M., Miró, E.E., 2005. Monolithic reactors for environmental applications: a review on preparation technologies. Chem. Eng. J. 109 (1), 11–36.
Azis, M.M., Auvray, X., Olsson, L., Creaser, D., 2015. Evaluation of H2 effect on NO oxidation over a diesel oxidation catalyst. Appl. Catal. B Environ. 179 (2), 542–550.
Bai, Q., Li, D., He, L., Xiao, H., Sui, N., Liu, M., 2015. Solvent-free selective hydrogenation of o-chloronitrobenzene to o-chloroaniline over alumina supported Pt nanoparticles. Prog. Nat. Sci. Mater. Int. 25 (3), 179–184.

Bogdan, E., Michorczyk, P., 2020. 3D printing in heterogeneous catalysis—the state of the art. Materials (Basel) 13 (20), 1–23.
Busse, C., Freund, H., Schwieger, W., 2018. Intensification of heat transfer in catalytic reactors by additively manufactured periodic open cellular structures (POCS). Chem. Eng. Process. Process. Intensif. 124, 199–214.
Cornejo, I., Nikrityuk, P., Hayes, R.E., 2020. The influence of channel geometry on the pressure drop in automotive catalytic converters: Model development and validation. Chem. Eng. Sci. 212, 115317.
El-Sayed, M.A., Essa, K., Ghazy, M., Hassanin, H., 2020. Design optimization of additively manufactured titanium lattice structures for biomedical implants. Int. J. Adv. Manuf. Technol. 110 (9–10), 2257–2268.
Essa, K., Hassanin, H., Attallah, M.M., Adkins, N.J., Musker, A.J., Roberts, G.T., et al., 2017. Development and testing of an additively manufactured monolithic catalyst bed for HTP thruster applications. Appl. Catal. A Gen. 542, 125–135.
Giani, L., Cristiani, C., Groppi, G., Tronconi, E., 2006. Washcoating method for Pd/γ-Al2O3 deposition on metallic foams. Appl. Catal. B Environ. 62 (1–2), 121–131.
Gremminger, A., Pihl, J., Casapu, M., Grunwaldt, J.D., Toops, T.J., Deutschmann, O., 2020. PGM based catalysts for exhaust-gas after-treatment under typical diesel, gasoline and gas engine conditions with focus on methane and formaldehyde oxidation. Appl. Catal. B Environ. 265, 118571.
Hajimirzaee, S., Doyle, A.M., 2020. 3D printed catalytic converters with enhanced activity for low-temperature methane oxidation in dual-fuel engines. Fuel 274, 117848.
Hajimirzaee, S., Shaw, D., Howard, P., Doyle, A.M., 2021. Industrial scale 3D printed catalytic converter for emissions control in a dual-fuel heavy-duty engine. Chem. Eng. Sci. 231.
Hamedi, M.R., Doustdar, O., Tsolakis, A., Hartland, J., 2021. Energy-efficient heating strategies of diesel oxidation catalyst for low emissions vehicles. Energy 230, 120819.
Hassanin, H., El-Sayed, M.A., Elshaer, A., Essa, K., Jiang, K., 2018. Microfabrication of net shape zirconia/alumina nanocomposite micro parts. Nanomaterials 8 (8).
Hassanin, H., Alkendi, Y., Elsayed, M., Essa, K., Zweiri, Y., 2020. Controlling the properties of additively manufactured cellular structures using machine learning approaches. Adv. Eng. Mater. 22 (3), 1–9.
Hassanin, H., Essa, K., Elshaer, A., Imbaby, M., El-Mongy, H.H., El-Sayed, T.A., 2021. Micro-fabrication of ceramics: additive manufacturing and conventional technologies. J. Adv. Ceram. 10 (1), 1–27.
Herreros, J.M., Gill, S.S., Lefort, I., Tsolakis, A., Millington, P., Moss, E., 2014. Enhancing the low temperature oxidation performance over a Pt and a Pt-Pd diesel oxidation catalyst. Appl. Catal. B Environ. 147, 835–841.
Ibrahim, H.A., Ahmed, W.H., Abdou, S., Blagojevic, V., 2018. Experimental and numerical investigations of flow through catalytic converters. Int. J. Heat Mass Transf. 127, 546–560.
Jung, Y., Pyo, Y.D., Jang, J., Kim, G.C., Cho, C.P., Yang, C., 2019. NO, NO2 and N2O emissions over a SCR using DOC and DPF systems with Pt reduction. Chem. Eng. J. 369 (2), 1059–1067.
Karatzas, X., Jansson, K., Dawody, J., Lanza, R., Pettersson, L.J., 2011. Microemulsion and incipient wetness prepared Rh-based catalyst for diesel reforming. Catal. Today 175 (1), 515–523.
Kim, J.Y., Son, S., 1999. Improving flow efficiency of a catalytic converter using the concept of radially variable cell density - part I. SAE Tech. Pap. Ser., 724
Klumpp, M., Körner, C., Inayat, A., Schwerdtfeger, J., Freund, H., Schwieger, W., et al., 2014. Periodic open cellular structures with ideal cubic cell geometry: effect of porosity and cell orientation on pressure drop behavior. Chem. Eng. J. 242, 364–378.
Kovacev, N., Li, S., Zeraati-Rezaei, S., Hemida, H., Tsolakis, A., Essa, K., 2020. Effects of the internal structures of monolith ceramic substrates on thermal and hydraulic properties: additive manufacturing, numerical modelling and experimental testing. Int. J. Adv. Manuf. Technol. 112, 1115–1132.
Kovacev, N., Li, S., Essa, K., 2021. Effect of the preparation techniques of photopolymerizable ceramic slurry and printing parameters on the accuracy of 3D printed lattice structures. J. Eur. Ceram. Soc. 41 (15), 7734–7743.
Kovacev, N., Li, S., Li, W., Zeraati-Rezaei, S., Tsolakis, A., Essa, K., 2022. Additive manufacturing of novel hybrid monolithic substrates. Aerospace 9 (225).
Lefort, I., Herreros, J.M., Tsolakis, A., 2014. Reduction of low temperature engine pollutants by understanding the exhaust species interactions in a diesel oxidation catalyst. Environ. Sci. Technol. 48 (4), 2361–2367.
Lucci, F., Della Torre, A., von Rickenbach, J., Montenegro, G., Poulikakos, D., Dimopoulos, E.P., 2014. Performance of randomized Kelvin cell structures as catalytic substrates: mass-transfer based analysis. Chem. Eng. Sci. 112, 143–151.
Lucci, F., Della Torre, A., Montenegro, G., Dimopoulos, E.P., 2015. On the catalytic performance of open cell structures versus honeycombs. Chem. Eng. J. 264, 514–521.
Megaritis A, Wyszynski ML, Tsolakis A, Cracknell R, Peucheret SM, Xu HM, et al. Exhaust gas fuel reforming for IC Engines using diesel type fuels. SAE Tech Pap Ser. 2010;1(x):1289–94
Olabi, A.G., Maizak, D., Wilberforce, T., 2020. Review of the regulations and techniques to eliminate toxic emissions from diesel engine cars. Sci. Total Environ. 748, 141249.
Papetti, V., Dimopoulos Eggenschwiler, P., Della Torre, A., Lucci, F., Ortona, A., Montenegro, G., 2018. Additive Manufactured open cell polyhedral structures as substrates for automotive catalysts. Int. J. Heat Mass Transf. 126, 1035–1047.
Papetti, V., Dimopoulos Eggenschwiler, P., Della Torre, A., Montenegro, G., Onorati, A., Ortona, A., et al., 2021. Instationary heat and mass transfer phenomena in additive manufactured open cell polyhedral structures for automotive catalysis. Chem. Eng. Sci. 234, 116448.
Piqueras, P., Ruiz, M.J., Herreros, J.M., Tsolakis, A., 2021. Influence of the cell geometry on the conversion efficiency of oxidation catalysts under real driving conditions. Energy Convers. Manag., 233
Resitoglu, I., Altinisik, K., Keskin, A., 2015. The pollutant emissions from diesel-engine vehicles and exhaust aftertreatment systems. Clean Techn. Env. Policy 17, 15–27.
Russell, A., Epling, W.S., 2011. Diesel oxidation catalysts. Catal. Rev. - Sci. Eng. 53 (4), 337–423.
Sabouri, A., Yetisen, A.K., Sadigzade, R., Hassanin, H., Essa, K., Butt, H., 2017. Three-dimensional microstructured lattices for oil sensing. Energy and Fuels 31 (3), 2524–2529.
Salomons, S., Votsmeier, M., Hayes, R.E., Drochner, A., Vogel, H., Gieshof, J., 2006. CO and H2 oxidation on a platinum monolith diesel oxidation catalyst. Catal. Today 117 (4), 491–497.
Santoliquido, O., Bianchi, G., Dimopoulos Eggenschwiler, P., Ortona, A., 2017. Additive manufacturing of periodic ceramic substrates for automotive catalyst supports. Int. J. Appl. Ceram. Technol. 14 (6), 1164–1173.
Santoliquido, O., Colombo, P., Ortona, A., 2019. Additive Manufacturing of ceramic components by digital light processing: a comparison between the "bottom-up" and the "top-down" approaches. J. Eur. Ceram. Soc. 39 (6), 2140–2148.
Theinnoi, K., Temwutthikun, W., Wongchang, T., Sawatmongkhon, B., 2018. Application of exhaust gas fuel reforming in diesel engines towards the improvement urban air qualities. Energy Procedia 152, 875–882.
Umar, M., Nozari, H., Menezes, M.R., Herreros, J.M., Lau, C.S., Tsolakis, A., 2021. Hydrogen production from bioethanol fuel mixtures via exhaust heat recovery in diesel engines: a promising route towards more energy efficient road vehicles. Int. J. Hydrogen Energy 46 (46), 23603–23614.
Zhu, J., Wu, P., Chao, Y., Yu, J., Zhu, W., Liu, Z., et al., 2022. Recent advances in 3D printing for catalytic applications. Chem. Eng. J. 433, (P1) 134341.